

ORIGINAL ARTICLE

Identification of a novel *TBX5* c.755 + 1 G > A variant and related pathogenesis in a family with Holt–Oram syndrome

De-Gang Wang^{1,2,3}  | Xing-Sheng Dong² | Yi Xiong^{2,3} | Zhi-Ming Li² | Ying-Jun Xie⁴ | Shu-Hua Liang³ | Tian-Hua Huang^{1,5}

¹Research Center for Reproductive Medicine, Shantou University Medical College, Shantou, China

²Prenatal Diagnosis Center, Boai Hospital of Zhongshan, Zhongshan, China

³The Second School of Clinical Medicine, Southern Medical University, Guangzhou, China

⁴Department of Obstetrics and Gynecology, Key Laboratory for Major Obstetric Diseases of Guangdong Province, The Third Affiliated Hospital of Guangzhou Medical University, Guangzhou, China

⁵Chengdu Jinxin Research Institute for Reproductive Medicine and Genetics, Chengdu, China

Correspondence

Tian-Hua Huang, Research Center for Reproductive Medicine, Shantou University Medical College, Shantou, Guangdong, China. Email: thuang@stu.edu.cn

Abstract

The proband with congenital heart disease and abnormal thumb was clinically diagnosed as Holt–Oram syndrome (HOS). A novel variant, T-box transcription factor 5 (*TBX5*) c.755 + 1 G > A, was identified in the proband via whole exome sequencing and validated using Sanger sequencing. Pedigree analysis and clinical examinations revealed three/seven individuals over three generations within the family, with features suggestive of HOS. Deep amplicon sequencing confirmed that the allele frequencies of the novel variant in the proband (III-1), her brother (III-2), and her mother (II-2) were 50%, 48.3%, and 38.1%, respectively, indicating that III-1 and III-2 harbored heterozygous variants, while II-2 harbored mosaic heterozygous variants. The minigene splicing assay showed that the novel variant affected the normal splicing of exon 7, resulting in the production of abnormal *TBX5* transcripts. Reverse transcription-quantitative polymerase chain reaction and western blot analyses revealed that the novel variant upregulated *TBX5* expression at the transcriptional and translational levels. Nuclear localization assay demonstrated impaired nuclear localization of the mutant *TBX5*. Cell viability assay revealed the inhibition of cell activity by the mutant *TBX5*. Our findings indicate that the novel variant was potentially induced HOS, probably by causing aberrant splicing, reducing the enrichment of nuclear *TBX5* protein, and inhibiting cellular proliferation.

KEYWORDS

aberrant splicing, Holt–Oram syndrome, minigene splicing assay, *TBX5*

1 | INTRODUCTION

Holt–Oram syndrome (HOS; OMIM: 142900) is an autosomal dominant disorder characterized by congenital heart defects (CHDs), with or without rhythm disturbances and radial defects. HOS is caused by pathogenic variants of the T-box transcription factor 5 (*TBX5*) gene (Vanlerberghe et al., 2019). The severity of symptoms in patients with HOS within a family varies considerably (Lehner et al., 2003), and the

severity of cardiac defects does not correlate with limb abnormalities (Newbury-Ecob et al., 1996). Human *TBX5* is localized on chromosome 12q24.1, spans more than 47 kb, and contains nine exons (Yi et al., 2000). *TBX5* is a transcription factor that plays a critical role in the development of heart and forelimbs. Several studies in animal models have confirmed the sensitivity of cardiac development to *TBX5* dosage (Bruneau et al., 2001; Chiavacci et al., 2012; Mori et al., 2006). The embryonic heart and forelimbs express high levels of *TBX5* (Naiche

This is an open access article under the terms of the Creative Commons Attribution-NonCommercial-NoDerivs License, which permits use and distribution in any medium, provided the original work is properly cited, the use is non-commercial and no modifications or adaptations are made.

© 2021 The Authors. *American Journal of Medical Genetics Part A* published by Wiley Periodicals LLC.

et al., 2005). In the heart, *TBX5* regulates the transcription of downstream genes, such as the atrial natriuretic factor (ANF) (natriuretic peptide A, NPPA), fibroblast growth factor 10, and connexin 40, by binding to the T-box binding elements (Boogerd et al., 2010; Bruneau et al., 2001; Ghosh et al., 2001), often in combination with the transcription factor NK2 homeobox 5 (NKX2-5) (Hiroi et al., 2001). Deficiency of *TBX5* results in the abnormal expression of its downstream genes and is associated with severe cardiac and forelimb abnormalities in patients with HOS. HOS-associated variants are distributed across all exons of *TBX5*, with the majority of them localized within the T-box DNA-binding domain (Mori & Bruneau, 2004). Recently, several non-coding variants of *TBX5*, present in the promoter (Shan et al., 2012), 3' untranslated (Wang et al., 2017), and enhancer regions (Smemo et al., 2012) were reported to be associated with CHDs.

Although exonic variants of *TBX5* have been identified, the association between intronic variants and HOS needs to be elucidated. In the present study, a novel heterozygous variant *TBX5* c.755 + 1 G > A (NM_000192.3), which co-segregated with HOS, was identified within a family. Further, the pathogenesis of abnormal mRNA splicing induced by the novel variant was analyzed. Based on the finding from the study, the novel variant was speculated to be responsible for the induction of HOS, as indicated by its ability to induce aberrant splicing and enhance the abnormal cytoplasmic translocation of mutant *TBX5* protein.

2 | MATERIALS AND METHODS

2.1 | Editorial policies and ethical considerations

Written informed consent was obtained from all participants. All protocols involving human subjects, used in this study, were approved by the Ethics Review Committee of Boai Hospital of Zhongshan (approval number: KY-2019-007-01). In addition, the study was in conformity with the World Medical Association's Declaration of Helsinki on ethical principles for medical research involving human subjects (World Medical Association, 2013).

2.2 | Cell lines, culture media, and culture conditions

The HEK293T, MCF-7, and HeLa cell lines were purchased from the China Center for Type Culture Collection (CCTCC, China). The cells were cultured, with the high-glucose Dulbecco's Modified Eagle Medium (DMEM; Gibco, USA) containing 10% fetal bovine serum (Gibco, USA) and 1% Penicillin–Streptomycin (Gibco, USA), in a constant temperature incubator at 37°C and 5% CO₂ with saturated humidity.

2.3 | Clinical details of the proband

The proband (28-month-old Chinese girl) with CHDs and an abnormal thumb was referred, for identification of a possible diagnosis, to Boai

Hospital of Zhongshan, where she underwent clinical examinations, including cardiac ultrasound, hand X-ray, and whole exome sequencing (WES). Candidate pathogenic variants of the disease were screened using bioinformatic analysis. Within the family, three out of seven individuals exhibited features suggestive of HOS and a clear autosomal dominant inheritance pattern, as per the results of pedigree analysis and clinical examinations (Figure 1). Subsequently, peripheral venous blood samples were collected from the three patients and the phenotypically normal family members, and genomic DNA was extracted from these samples. To explore the possible pathogenesis of HOS caused by the novel variant, a series of molecular biological tests were performed, including a minigene splicing assay, reverse transcription-quantitative polymerase chain reaction (RT-qPCR), western blot, and nuclear localization assay.

2.4 | Library preparation and next-generation sequencing

Library preparation and next-generation sequencing (NGS) were performed at the Beijing Genomics Institute (BGI), China. Genomic DNA was extracted from 300 µl of venous blood collected from the proband (III-1) using the MagPure Buffy Coat DNA Midi KF Kit (Magen, China) according to the manufacturer's instructions. To generate short DNA fragments (100–500 bp), the extracted genomic DNA was fragmented using segmentase (BGI, China) and screened with magnetic beads to enrich the fragments with sizes ranging from 280 to 320 bp. Subsequently, the ends were filled and the base “Adenine” was added to the 3' end to facilitate ligation of the DNA fragment to the adapter with a “Thymine” base at the 5' end. A library was constructed using the purified DNA fragments amplified via a ligation-mediated polymerase chain reaction (PCR). The library was enriched by array hybridization, according to the manufacturer's instructions (Roche NimbleGen, USA), eluted, and amplified postcapture. The magnitude of enrichment in products was estimated using an Agilent 2100 Bioanalyzer. All amplified libraries were subsequently sent to the BGI for circularization and sequencing on the MGISEQ-2000 platform using a paired-end 100 bp sequencing strategy. The sequencing reads were automatically demultiplexed using the index.

2.5 | Bioinformatic analysis

“Clean reads” were generated using the filtering criteria published previously (Wei et al., 2011). These reads were mapped to the human reference genome (hg19) using the Burrows-Wheeler Aligner software (Li & Durbin, 2009). The output files from alignment were further subjected to sequencing coverage and depth analyses of the target region, single-nucleotide variants (SNVs), and insertions and deletions (indels) calling. SNVs and indels were detected using the Genome Analyses Tool Kit and filtered and assessed using multiple databases, including, dbSNP, HapMap, 1000 Genome database, and a

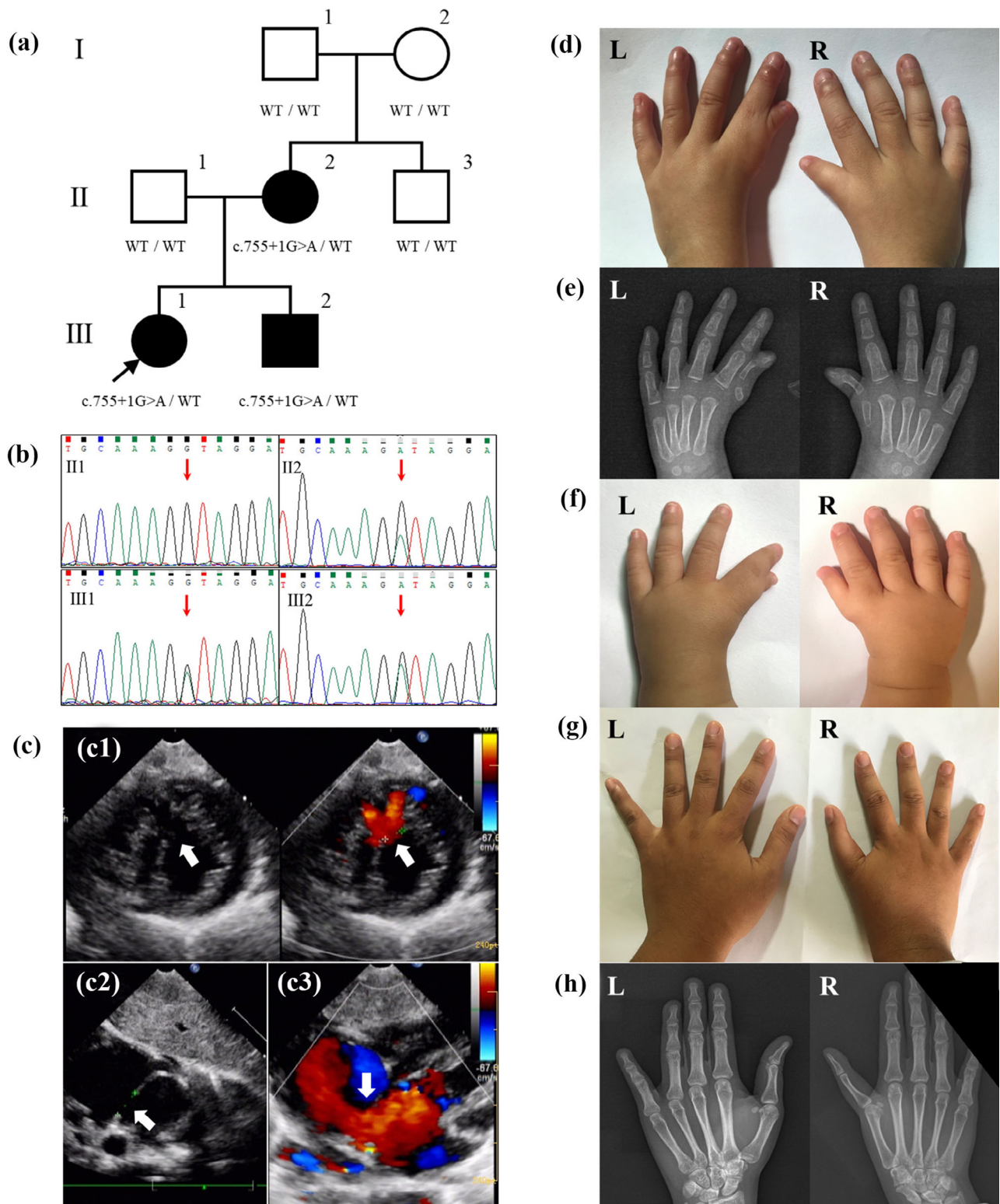


FIGURE 1 *TBX5* c.755 + 1G > A was detected in a Chinese family with Holt-Oram syndrome. (a) Pedigree of the family indicating the proband (arrow; III-1), her younger brother (III-2), and her mother (II-2), who harbored heterozygous variant and were affected by Holt-Oram syndrome. (b) The results of Sanger sequencing for II-1, II-2, III-1, and III-2. The red arrow indicates the site of wild-type (II-1) and heterozygous variant (II-2, III-1, and III-2). (c) Echocardiographic findings of III-1. (c1) The largest ventricular septal defect was approximately 5.2 mm (arrow). (c2) The location of the atrial septal defect was approximately 10.2 mm (arrow). (c3) Left to right shunt caused by the atrial septal defect. (d,e) Images and X-ray scans of III-1-hands showed the presence of thenar hypoplasia, thumb hypoplasia, I-II-syndactyly and first metacarpal agenesis. (f) Images of III-2-hands showed the presence of malformations similar to those observed in III-1. (g,h) Images and X-ray scans of the hands of II-2 mostly indicated normal features

database of 100 healthy Chinese adults. The effects of the variants were predicted using Scale-invariant feature transform and Poly-Phen2. Variants were evaluated according to the protocol issued by the American College of Medical Genetics (ACMG) (Richards et al., 2015). Mutations reported in the published studies were screened using the Human Gene Mutation Database (HGMD).

2.6 | Deep amplicon sequencing

Deep amplicon sequencing was performed at Guangzhou Jiajian Medical Testing Co., Ltd., China, using custom-designed probe libraries targeting *TBX5*, and the sequence data were analyzed on a HiSeq 2000 sequencer (Illumina, USA) according to the manufacturer's instructions. Sequence data were demultiplexed using Casava (version 1.7; Illumina) and processed further for alignment using NextGENe (version 4.0.5; SoftGenetics, USA). The mean sequence coverage per base was $> 5000\times$. All variant calls were reviewed and confirmed with Sanger sequencing. An in-house bioinformatic pipeline was used for variant detection and annotation, as described previously (Qin et al., 2016).

2.7 | Sanger sequencing

To validate and detect the novel variant *TBX5* c.755 + 1 G > A (NM_000192.3) in the proband (III-1) and the family members (I-1, I-2, II-1, II-2, II-3, and III-2), conventional Sanger sequencing was performed at BGI, China.

2.8 | Plasmid construction and transfection

For the minigene splicing assay, the entire exon 7 and surrounding intron 7 sequence of wild-type and mutant *TBX5* were cloned into a splicing reporter plasmid, namely, the pcMINI-N vector containing the sequence of IntronB-ExonB (Bioeagle, China) to construct pcMINI-N-*TBX5*^{wt} and pcMINI-N-*TBX5*^{mut}, respectively. The nucleotide sequences of the primers used for *TBX5* amplification are listed in Table S1. pcMINI-N-*TBX5*^{mut} and pcMINI-N-*TBX5*^{wt} were transfected into the HEK293T and MCF-7 cells, respectively, using Metafectene (Biontix, Germany) following the manufacturer's instructions.

To evaluate the effect of the variant on *TBX5* transcription and translation, full-length *TBX5* cDNA was cloned into the plasmids pEGFP-C1 and pHAGE to construct pEGFP-C1-*TBX5*^{wt} and pHAGE-*TBX5*^{wt}, respectively. The *TBX5* cDNA sequence, c.755_756ins56bp, deciphered using the minigene splicing assay, was inserted into the above-mentioned recombination vectors, using site-directed mutagenesis to construct pEGFP-C1-*TBX5*^{mut} and pHAGE-*TBX5*^{mut}, respectively. The wild-type and mutant vectors were transfected into HEK293T cells using Lipofectamine 2000 according to the manufacturer's instructions (Yeasen Biotech, China).

2.9 | Minigene splicing assay

Total RNA was extracted from HEK293T and MCF-7 cells at 48 h post-transfection using TRIzol reagent (Takara, Japan). The extracted RNA was treated with DNase I (Thermo Scientific, USA) and reverse transcribed using the ImProm-II™ Reverse Transcription System according to the manufacturer's instructions (Promega, USA). To detect the alterations in splicing, minigene-specific cDNA was amplified using plasmid-specific primers (Table S2). The PCR products were separated using 12% agarose gel electrophoresis (AGE). To characterize the splicing pattern, the PCR products were subjected to Sanger sequencing.

2.10 | Reverse transcription-quantitative polymerase chain reaction

To examine the effect of the variant on the transcriptional level of *TBX5*, total RNA was extracted from the cells transfected with recombinant plasmids containing wild-type and mutant *TBX5* cDNA, treated with DNase I, and reverse transcribed as described above for the minigene splicing assay. The nucleotide sequences of primers used to quantitate the transcription of wild-type and mutant *TBX5* using RT-qPCR are listed in Table S3. β -actin was used as an internal control. RT-qPCR was performed using a 7500HT Fast RT-PCR instrument (Life Technologies, USA). The cycling conditions were as follows: 95°C for 3 min, followed by 45 cycles at 95°C for 15 s, and 60°C for 30 s. Data were analyzed quantitatively using the $2^{-\Delta\Delta Ct}$ method.

2.11 | Western blot analysis

To evaluate the effect of the variant on the translational level of *TBX5*, protein samples of the cells transfected with the recombinant constructs containing wild-type and mutant *TBX5* cDNA were resolved using 10% sodium dodecyl sulfate polyacrylamide gel electrophoresis and were further electroblotted onto a polyvinylidene difluoride membrane (Beyotime, China). The membranes were incubated overnight at 4°C with mouse anti-green fluorescent protein (GFP), anti-hemagglutinin (HA), or anti- β -actin primary antibodies (BioVision, USA) to facilitate the formation of specific immune complexes. After incubation, the membranes were washed and incubated with a horseradish peroxidase-conjugated goat anti-mouse IgG secondary antibody at room temperature for 1 h. Immunoreactive protein bands were detected using a chemiluminescence imaging analysis system, according to the manufacturer's instructions (Syngene, USA).

2.12 | Nuclear localization assay

Immortalized HeLa cells were seeded on cover slips, at a density of 5×10^5 cells/well in standard 12-well plates. The cells were 40%–50% confluent and then transfected with the recombinant plasmids

pHAGE-TBX5^{wt} and pHAGE-TBX5^{mut} using Lipofectamine 2000 according to the manufacturer's instructions. At 48 h post-transfection, the cells were fixed in 2% paraformaldehyde, permeabilized with 0.3% Triton X-100, and incubated with a mouse anti-TBX5 (1:100; Proteintech, USA) antibody at 4°C for 24 h and an Alexa488-conjugated rabbit anti-mouse antibody (1:200; Invitrogen, USA) at room temperature for 2 h. Immunofluorescence signals were visualized under a fluorescence microscope (Life Technologies). Photoshop CC 2019 was used to measure the cytoplasmic and nuclear fluorescence signals.

2.13 | Cell viability assay

HeLa cells were seeded in triplicate, at a density of 1×10^4 cells/well, in 96-well plates. Cell adhesion and proliferation were evaluated by assessing cell viability using a commercial cell counting kit-8 (CCK-8; Biosharp, China) according to the manufacturer's instructions. After incubating the cells overnight at 37°C, 100 μ l each of the pHAGE-TBX5^{wt}/liposome and pHAGE-TBX5^{mut}/liposome complexes were added and incubated at 37°C for 24 and 48 h, respectively. Absorbance was measured at 450 nm using a microplate reader (TECAN, Switzerland) and the percentage of cell viability was calculated using the following formula: percentage of cell viability = $(A_{\text{treatment}} - A_{\text{blank}})/(A_{\text{control}} - A_{\text{blank}}) \times 100\%$, where A represents absorbance (Park & Xian, 2015).

2.14 | Statistical analysis

To determine the significant differences in the average transcriptional levels between the mutant and wild-type *TBX5* groups using $2^{-\Delta\Delta C_t}$ analysis, individual data were converted into a linear form using the 2^{-C_t} calculation method (Livak & Schmittgen, 2001) and then subjected to a paired-sample t-test using the SPSS software (version 16.0). Significant differences in the average translational level and cell viability between the mutant and wild-type *TBX5* groups were determined using the Student's *t*-test. Significant differences in the percentage of cells exhibiting nuclear *TBX5* expression between mutant and wild-type *TBX5* groups were measured using the Chi-square test. Statistical significance was set at $p < 0.05$.

3 | RESULTS

3.1 | Varied clinical phenotypes of patients with HOS

The family analyzed for HOS had three affected and four unaffected members (Figure 1a). The proband (III-1) presented with CHD, including cor triatriatum sinistrum, atrial septal defect, ventricular septal defect, tricuspid regurgitation, and pulmonary hypertension, as well as upper limb malformations, including thenar and thumb hypoplasia, I-II

syndactyly, first metacarpal agenesis, and limitation of thumb bending (Figure 1c–e). The younger brother of proband (III-2) presented with atrial septal defect, tricuspid regurgitation, pulmonary hypertension, left superior vena cava, thenar hypoplasia, thumb hypoplasia, I-II syndactyly, first metacarpal agenesis, and limitation of thumb bending (Figure 1f). The mother of proband (II-2) was diagnosed with thenar hypoplasia and limitation of thumb bending (Figure 1g). Significant abnormalities were not detected in the mother's palm, as indicated by the results of palm radiography (Figure 1h). The diverse clinical manifestations among affected members are summarized in Table 1. The father, uncle, and grandparents (II-1, II-3, I-1, and I-2) of the proband did not exhibit symptoms of CHDs or abnormalities of the upper limb.

3.2 | A novel likely pathogenic variant identified using WES

The genetic cause of HOS in the family was determined by performing WES of the proband (III-1). WES generated and aligned 21.47 billion bases of the sequence to those of hg19. The bases were mapped to the targeted bases with an average depth of 147.15-fold and a coverage rate of 99.76%. A total of 23,067 SNVs and indels were detected in 5700 candidate genes. A heterozygous variant c.755 + 1 G > A was detected at the splicing site of *TBX5* (NM_000192.3). Further validation using Sanger sequencing confirmed the presence of the heterozygous variant in the affected members III-1, II-2, and III-2 (Figure 1b). Further, the heterozygous variant was not detected in the unaffected family members (II-1, II-3, I-1, and I-2) (Figure 1b; Figure S1). Therefore, the c.755 + 1 G > A variant in *TBX5* co-segregated with the HOS phenotype in the family. According to the guidelines for the interpretation of sequence variants, issued by ACMG (Richards et al., 2015), *TBX5* c.755 + 1 G > A can be classified as a likely pathogenic variant based on the evidence of PVS1 and PM2.

3.3 | Confirmation of allele frequency using deep amplicon sequencing

The allele frequency (AF) of *TBX5* c.755 + 1 was evaluated using capture-based NGS with custom-designed probe libraries. The AFs of *TBX5* c.755 + 1 G > A in the proband (III-1), her brother (III-2), and her mother (II-2) were found to be 50% (G/A: 7952/7950), 48.3% (G/A: 4822/5165), and 38.1% (G/A: 2413/3924), respectively (Table S4), indicating that III-1 and III-2 harbored a heterozygous variant, whereas II-2 harbored a mosaic heterozygous variant.

3.4 | The variant caused retention of intron 7 (56 bp)

The entire exon 7 and surrounding intron 7 of wild-type and mutant *TBX5* were cloned into a report vector, pcMINI-N, which was used to transfect HEK293T and MCF-7 cells, respectively (Figure 2a). AGE of the

TABLE 1 Clinical manifestations of the affected individuals in a family with Holt–Oram syndrome

	III-1	III-2	II-2
Gender	Female	Male	Female
Age	2 years 4 months	6 months	31 years
<i>TBX5</i> c.755 + 1 G > A	Het	Het	Mosaic Het
Variant AF (%)	50.0	48.3	38.1
Congenital heart disease (CHD)	+	+	–
Atrial septal defect (ostium secundum type)	+	+	–
Ventricular septal defect	+	–	–
Tricuspid regurgitation	+	+	–
Ductus arteriosus	+	–	–
Cor triatriatum	+	–	–
Pulmonary hypertension	+	+	–
Left superior vena cava	–	+	–
Conduction disturbances	–	–	–
Hand	+	+	+
Thenar hypoplasia	+	+	+
Thumb hypoplasia	+	+	–
I-II syndactyly	+	+	–
First metacarpal agenesis	+	+	–
Limitation of thumb bending	+	+	+
Forearm	–	–	–
Arm	–	–	–
Shoulder	–	–	–

Abbreviations: AF, allele frequency; Het, heterozygous; *TBX5*, T-box transcription factor 5; III-1, proband; III-2, younger brother of the proband; II-2, mother of the proband.

RT-PCR fragments generated from minigene-spliced RNA of the wild-type and mutant constructs revealed that the wild-type construct formed the expected band size (band a), while the mutant construct formed a larger DNA band (band b) (Figure 2b). Sanger sequencing indicated a normal splicing pattern in band a [Exon7(92 bp)-ExonB], while the retention of a partial intron 7 (56 bp) that altered the splicing pattern [Exon7 (92 bp)-∇intron7(56 bp)-ExonB] was observed in band b (Figure 2c). The results obtained from the HEK293T and MCF-7 cells were consistent, suggesting that the effect on the splicing of *TBX5* mRNA was independent of the cell type. The results showed that the *TBX5* c.755 + 1 G > A variant induced an abnormal splicing pattern with intron retention, as a partial intron 7 (56 bp) was retained between exons 7 and 8 (c.755_756ins56bp) in vitro. Intron retention led to the substitution of serine with arginine at the 252nd amino acid in *TBX5*, resulting in the formation of a premature termination codon (PTC). Therefore, the *TBX5* c.755 + 1 G > A variant disrupted normal *TBX5* expression by forming a truncated *TBX5* protein (p. S252Rfs*2, Figure 2d).

3.5 | The variant enhanced the mRNA and protein expression of *TBX5*

To investigate the effect of the *TBX5* c.755 + 1 G > A variant on the mRNA and protein expression of *TBX5*, the recombinant

plasmids pEGFP-C1-*TBX5*^{wt}, pHAGE-*TBX5*^{wt}, pEGFP-C1-*TBX5*^{mut}, and pHAGE-*TBX5*^{mut} were constructed and transfected into HEK293T cells. The RT-qPCR results showed significantly enhanced mRNA expression of the mutant compared to that of wild-type *TBX5* in HEK293T cells ($p < 0.05$; Figure 3a,b). Western blot results revealed the synthesis of a truncated protein, with lower molecular weight, from mutant *TBX5*. In addition, a significantly higher expression of the truncated protein than that of wild-type *TBX5* protein was observed ($p < 0.05$, Figure 3c–f). Collectively, these results indicated that the variant *TBX5* c.755 + 1 G > A could enhance the mRNA and protein expression of *TBX5* in vitro.

3.6 | Impaired nuclear localization of the truncated *TBX5*

To investigate the cellular localization of the truncated *TBX5* protein, HeLa cells were transfected with the pHAGE-*TBX5*^{wt} and pHAGE-*TBX5*^{mut} constructs. Immunofluorescence staining revealed the altered nuclear localization of the truncated *TBX5* protein. The wild-type *TBX5* protein was significantly localized in the nucleus, whereas the truncated *TBX5* protein was found to be dispersed both in the cytoplasm and in the nucleus

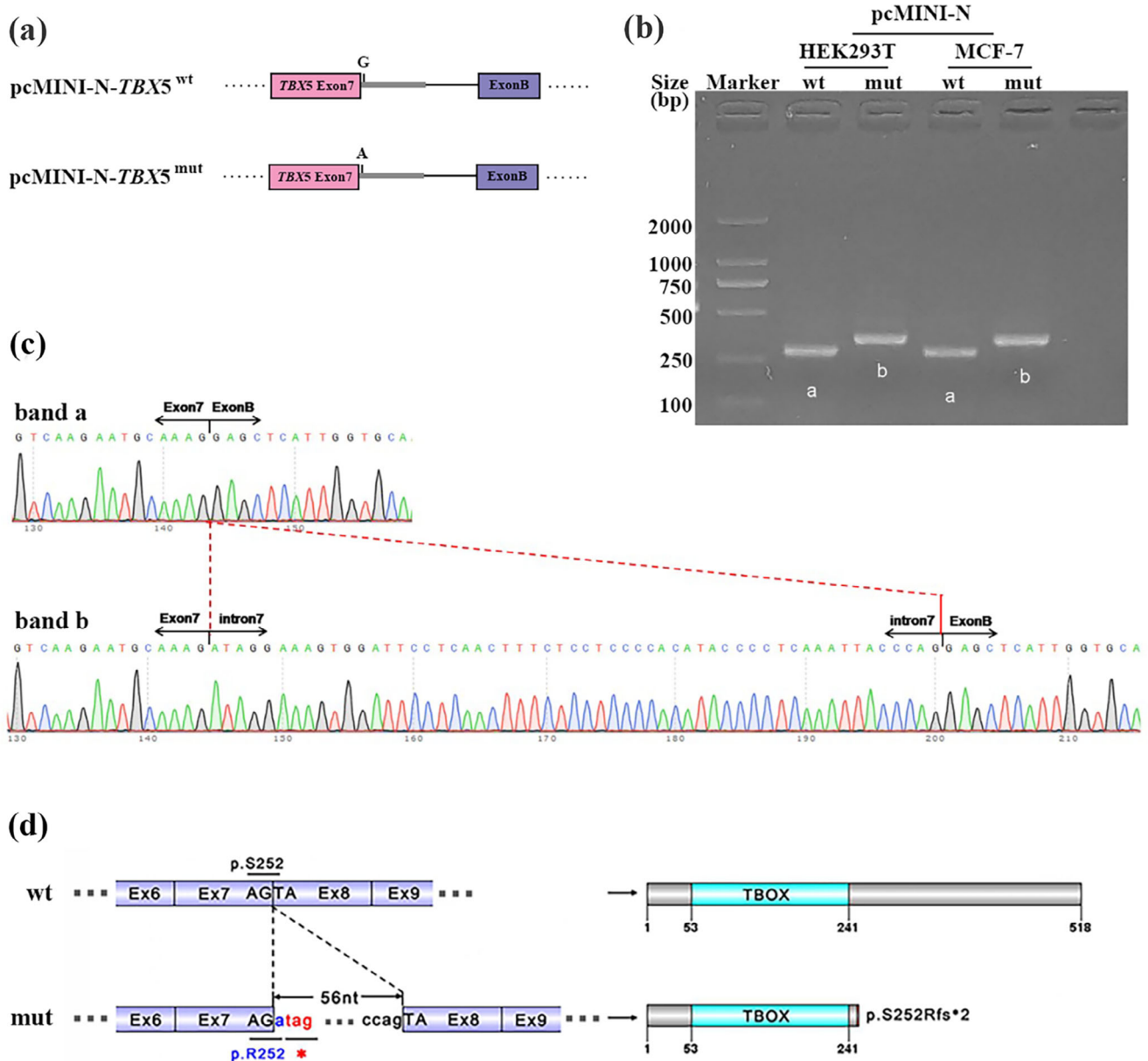


FIGURE 2 Results of the minigene splicing assay for *TBX5* c.755 + 1 G > A in HEK293T and MCF-7 cells. (a) In the minigene splicing assay, the entire exon 7 and surrounding intron 7 (thick gray line) of human *TBX5* were cloned into pcMINI-N vector containing the intron B (thin black line) and exon B sequence. Comparing with pcMINI-N-*TBX5*^{wt} construct, the original base “Guanine” is replaced by the base “Adenine” at the first nucleotide position of intron 7 of *TBX5* in pcMINI-N-*TBX5*^{mut}. (b) pcMINI-N-*TBX5*^{mut} and pcMINI-N-*TBX5*^{wt} were transfected into HEK293T and MCF-7 cells, respectively, and following which RT-PCR was performed. The results showed that the band size of pcMINI-N-*TBX5*^{wt} s in HEK293T or s MCF-7 cells (band a) was approximately 289 bp, as expected, and that of pcMINI-N-*TBX5*^{mut} in both cell lines (band b) was considerably larger. This indicated that the transcript of pcMINI-N-*TBX5*^{mut} was altered compared to that of pcMINI-N-*TBX5*^{wt}. (c) Sanger sequencing demonstrated that the band a exhibited a normal splicing pattern of the mRNA [exon 7-exon B], while the band b exhibited an erroneous splicing pattern; therefore, the *TBX5* c.755 + 1 G > A variant may have affected the normal splicing pattern of exon 7, resulting in the retention of a 56 bp in part of intron 7 and the generation of abnormal *TBX5* mRNA transcript [exon 7-∇intron 7 (56 bp)-exon B]. (d) Based on the above findings, it was presumed that the retention of a part of intron 7 resulted in the substitution of the 252nd amino acid, serine (p.S252), of *TBX5* with arginine (p.R252), and the introduction of a premature termination codon, leading to the generation of the truncated *TBX5* protein (p.S252Rfs*2)

(Figure 4). A greater proportion of nuclear localization was observed in the wild-type *TBX5* protein than in the truncated *TBX5* protein (36% vs. 15%, $p = 0.000$; Table 2). Therefore, the truncated *TBX5* protein possibly exhibited impaired nuclear localization in vitro.

3.7 | Truncated *TBX5* inhibited the proliferation of HeLa cells

A cell proliferation assay was used to analyze the effect of truncated *TBX5* on cell viability. HeLa cells were transfected with the pHAGE-*TBX5*^{wt}

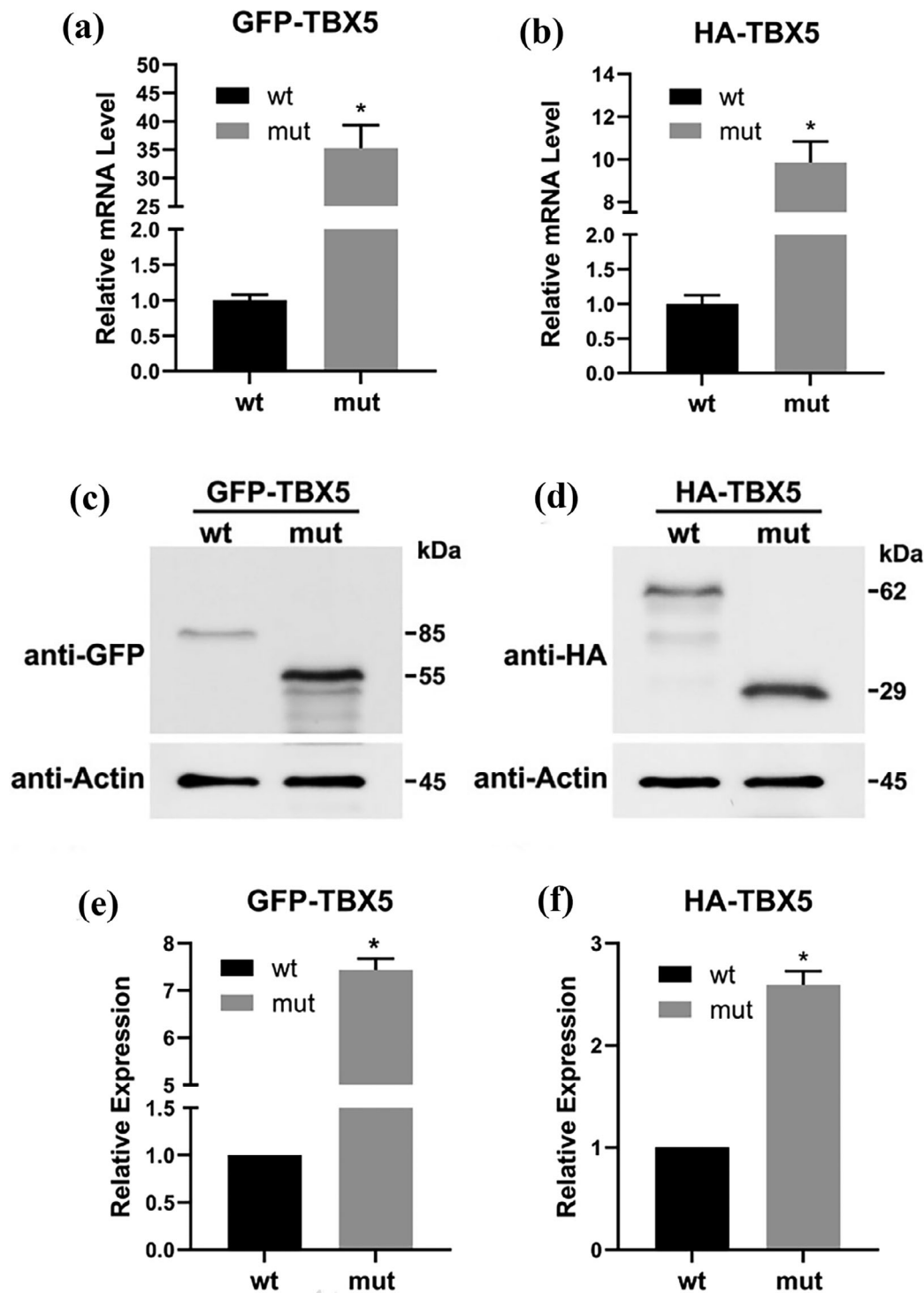


FIGURE 3 *TBX5* c.755 + 1 G > A increased the level of *TBX5* mRNA and protein. To examine whether the variant affected the *TBX5* transcriptional and translational levels, full-length *TBX5* cDNA was cloned into the plasmid pEGFP-C1 and pHAGE to construct the recombinant vectors pEGFP-C1-*TBX5*^{wt} (GFP-*TBX5*^{wt}) and pHAGE-*TBX5*^{wt} (HA-*TBX5*^{wt}), respectively; based on the results of minigene splicing assay, the *TBX5* cDNA sequence of c.755_756ins56bp was inserted into the above vectors to construct pEGFP-C1-*TBX5*^{mut} (GFP-*TBX5*^{mut}) and pHAGE-*TBX5*^{mut} (HA-*TBX5*^{mut}), respectively. The wild-type (wt) and mutant-type (mut) vectors were then transfected into HEK293T cells. (a,b) The RT-qPCR results showed that the mRNA level of mutant *TBX5* was significantly higher than that of wild-type *TBX5* in HEK293T cells. * Represents $p < 0.05$. (c,d) Western blot showed that the molecular weight of the mutant protein in the GFP-*TBX5*^{mut} and HA-*TBX5*^{mut} groups was considerably lower than that of the wild-type protein in the GFP-*TBX5*^{wt} and HA-*TBX5*^{wt} groups, which indirectly confirmed that the mutant *TBX5* was truncated compared to wild-type *TBX5*. Actin was selected as an internal control. (e,f) Quantitating the levels of the mutant and wild-type *TBX5* proteins by densitometry analysis of western blot. The translational level of mutant *TBX5* was significantly higher than that of wild-type *TBX5*. * Represents $p < 0.05$

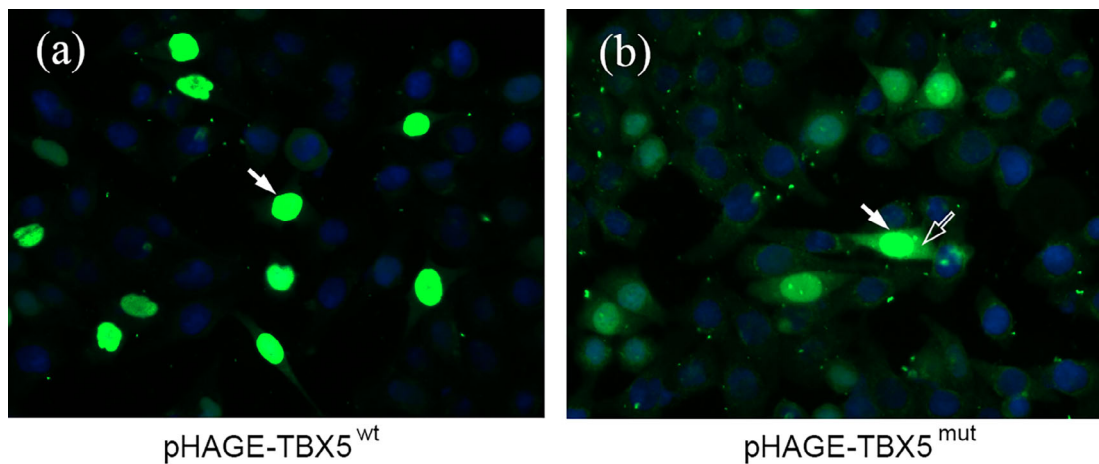


FIGURE 4 *TBX5* c.755 + 1 G > A variant altered the nuclear localization of TBX5. The recombinant vectors pHAGE-TBX5^{wt} and pHAGE-TBX5^{mut} were transfected into immortalized HeLa cells. Immunofluorescence staining revealed that the wild-type TBX5 was almost exclusively expressed in the nucleus (white arrow in (a)), whereas the mutant TBX5 was localized both in the cytoplasm (hollow arrow in (b)) as well as the nucleus (white arrow in (b))

TABLE 2 Number of cells with TBX5 protein located in the nucleus

Types of vector	Total no. of cells	No. of cells with TBX5 in nucleus	Percentage (%)	χ^2 value	<i>p</i> value
pHAGE-TBX5 ^{wt}	386	140	36.3	44.76	0.000
pHAGE-TBX5 ^{mut}	528	89	16.9		

and pHAGE-TBX5^{mut} constructs. At 24 and 48 h post-transfection, cell viability was measured. Significant differences were not detected in the cell viabilities between the pHAGE-TBX5^{wt} and pHAGE empty groups. However, the cell viability was significantly lower (approximately 10%) in pHAGE-TBX5^{mut} cells than in pHAGE-TBX5^{wt} cells (Figure 5). Therefore, the truncated TBX5 protein probably inhibited cell proliferation in vitro.

4 | DISCUSSION

In the present study, a novel variant *TBX5* c.755 + 1 G > A was identified in an HOS family. This variant has not been reported in any of the reference population gene databases, including the International Genome Sample Resource (IGSR, 2021; accessed March 15, 2021), the Genome Aggregation Database (2021) (gnomAD, accessed March 15, 2021), ClinVar database (2021) (ClinVar, accessed March 15, 2021), and HGMD (2021) (accessed March 15, 2021), which are used to screen pathogenic variants reported in published studies. Although the novel *TBX5* variant was detected in the proband (III-1), her brother (III-2), and her mother (II-2), it was a de novo mosaic variant in II-2 but a maternal heterozygous variant in III-1 and III-2, as the AF in II-2 was 38.08% and approximately 50% in III-1 and III-2 (50.01% and 48.28%, respectively). Previous studies have shown that patients with mosaic variants exhibit various clinical symptoms, such as early pregnancy loss, organ-specific pathologies, and modification of clinical syndromes, depending on the type of variant, the proportion of cells harboring the variant, and the tissue distribution of the

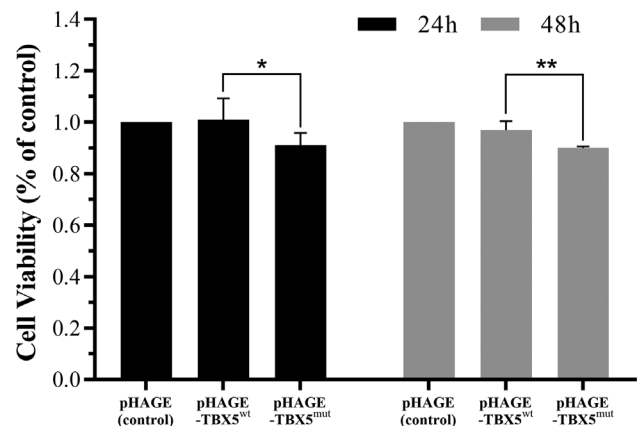


FIGURE 5 Comparison of HeLa cell viability among the groups transfected with empty pHAGE, pHAGE-TBX5^{wt}, and pHAGE-TBX5^{mut}. The results of the cell viability assay indicated that the average absorbance value of the cells in the pHAGE-TBX5^{mut} group was significantly lower than that in the pHAGE-TBX5^{wt} group after incubation for 24 and 48 h ($n = 6$). This suggested that the mutant TBX5 probably inhibited the cell viability in vitro. * Represents $p < 0.05$, ** Represents $p < 0.01$

genetic change (Spinner & Conlin, 2014). In the present study, compared to III-1 and III-2, who harbored the heterozygous variant, II-2 exhibited no obvious abnormalities in the heart and hands, except for the limitation of thumb bending and thenar hypoplasia. However, the absence of an obvious clinical phenotype is not a common feature in

patients harboring mosaic variants. Owing to the phenotypic diversity, mosaic variants were detected in individuals with normal phenotypes, such as the mother of the proband in the present study and the proband's mother or father in the previous study (Carvill et al., 2013), as well as in the patients exhibiting different clinical phenotypes, such as patients with tuberous sclerosis complex with different affected organs and clinical symptoms owing to varying levels of mosaicism, as reported in a previously published study (Tyburczy et al., 2015). Based on the calculations derived from the variant's AF (38.08%) in II-2, approximately 76% of the cells in the peripheral blood were heterozygous for the *TBX5* c.755 + 1 G > A variant, and the remaining 24% of the cells expressed the wild-type protein. Importantly, II-2 had two affected children (III-1 and III-2), indicating the presence of the variant in her germ cells. Therefore, II-2 should be medically advised to undergo preimplantation and prenatal genetic diagnosis for *TBX5*, if and when she prepares for her next pregnancy.

HOS is an autosomal dominant condition with complete penetrance. However, the expressivity may vary based on the variability of the severity of clinical manifestations among affected members harboring the same *TBX5* variant. In the present study, the varying severity of clinical phenotypes between the proband and her brother, both harboring the same heterozygous variant, may be explained based on the varied HOS expressivity.

The human *TBX5* protein is primarily expressed in the heart, placenta, lungs, and esophagus but not in the blood (GTEx Consortium, 2020; Hatcher et al., 2000; Mele et al., 2015). Hence, to verify mRNA splicing, it is practically impossible to collect samples of tissues with *TBX5* expression from patients with HOS. Therefore, an in vitro minigene splicing assay was performed to study the pathogenic mechanism of the variant at the splice site, as its accuracy and dependability have been demonstrated in previous studies (Merico et al., 2020; Qiu et al., 2020; Wang et al., 2019). In the present study, the in vitro minigene splicing assay showed that the *TBX5* c.755 + 1 G > A variant altered the normal splicing of exon 7, resulting in the retention of a partial intron 7 (56 bp) and the production of an abnormal *TBX5* transcript. Further analyses and western blot revealed that the abnormal transcript altered the reading frame of the protein, thereby forming a PTC at the latter end of exon 7 and synthesizing a *TBX5* protein variant truncated at the 252nd amino acid. *TBX5*, through its interaction with the nucleosome remodeling and deacetylase (NuRD) complex and other transcriptional repressors, such as spalt-like transcription factor 4 (*SALL4*), remodels chromatin to a closed state, which inhibits the expression of noncardiac genes (Boogerd & Evans, 2016). The 252nd position is located in the NuRD interaction domain (NID), which is a domain consisting of 100 amino acids located near the T-box. We speculated that the variant-induced truncation of *TBX5* probably altered the function of NID, thereby affecting the ability of *TBX5* to interact with DNA and other transcription factors, such as *SALL4*.

Nonsense-mediated mRNA decay (NMD) is a translation-dependent mRNA monitoring mechanism in eukaryotes that helps maintain the quality of gene expression. NMD scrutinizes newly synthesized mRNAs and degrades those that contain PTC, thereby

preventing the production of truncated proteins that might cause diseases in humans (Hug et al., 2016; Kurosaki & Maquat, 2016). You et al. reported that PTC within 50–55 nucleotides at the terminal exon–exon junction is not recognized by NMD and, therefore, certain mRNAs containing PTC could escape from the NMD system (You et al., 2007). Guo et al. identified a novel heterozygous splicing variant (c.1284 + 2del) in intron 4 of the exostosin glycosyltransferase 1 (*EXT1*) gene that caused a significant increase in the transcription and translation of the mutant compared to that of the wild-type *EXT1*. The authors deciphered that the deletion of exon 4 in *EXT1* introduced splicing abnormalities that eluded the NMD monitoring mechanism (Guo et al., 2019). In the present study, the *TBX5* c.755 + 1 G > A variant led to mRNA splicing abnormalities that escaped NMD monitoring and was translated into a truncated *TBX5* protein. Therefore, the mRNA and protein expression of *TBX5* was enhanced. However, the mechanism underlying the escape of the abnormal mRNA from NMD scrutiny needs to be elucidated in future studies.

The ubiquitin–proteasome system (UPS) is a post-transcription quality control system responsible for the degradation of proteins in eukaryotic cells (Pohl & Dikic, 2019) and plays a crucial role in biological processes integral to the development of the cardiovascular system and cardiovascular diseases (Willis et al., 2010). The UPS typically recognizes specific protein substrates and attaches polyubiquitin chains at lysine residues for subsequent degradation of the protein substrates by proteasomes. The amino acids at positions 244–518 in *Tbx5* were found to be responsible for the association with *Fbxo25*, an F-box containing protein that acts as an ubiquitin E3 ligase to degrade cardiac proteins via the ubiquitin pathway (Jang et al., 2011; Jeong et al., 2015). In the absence of the sequence recognized by the UPS, the mutant *TBX5* protein probably formed a truncated C-terminal segment from the 252nd amino acid, which made it difficult for ubiquitin E3 ligase to recognize the sequence, resulting in decreased degradation by the proteasome and increased half-life of the mutant *TBX5* protein. This explains, at least in part, why the mutant *TBX5* protein was expressed at higher levels in cultured cells compared to its wild-type counterpart.

Previous studies have demonstrated the localization of *TBX5* to the nucleus during embryogenesis, suggesting that altered nuclear localization may be related to disease pathogenesis (Collavoli et al., 2003). In the present study, the results of immunofluorescence assay revealed the significantly decreased nuclear localization of the truncated *TBX5* protein compared to that of the wild-type *TBX5* protein. The reduced localization of truncated *TBX5* may result from the cumulative effect of two factors. First, the *TBX5* protein contains two nuclear localization sequences (NLS): NLS1 located in the T-box domain (78–90 amino acid residues), and NLS2 located in the C-terminal region of the *TBX5* protein, outside the T-box domain (325–340 amino acid residues) (Zaragoza et al., 2004). NLS1 and NLS2 can function independently or collectively to localize *TBX5* to the nucleus. While NLS are incapable of promoting complete nuclear localization of *TBX5* individually, they can accomplish this synergistically (Collavoli et al., 2003). Accordingly, the loss of NLS2 in the truncated *TBX5* may

have reduced the intranuclear transfer of TBX5. Second, the histone acetyltransferases KAT2A and KAT2B interact with TBX5 and acetylate it at Lys339. Acetylation enhances the transcriptional activity of myosin heavy chain 6 and ANF, thereby promoting the nuclear localization of TBX5 (Ghosh et al., 2018). The Lys339 acetylation site is located within NLS2. In the present study, the lack of acetylation owing to the loss of NLS2 in the truncated TBX5 protein may have inhibited the nuclear transfer of TBX5.

The results of the cell viability assay indicated the decreased proliferation (10% at 24 and 48 h) of the HeLa cells transfected with pHAGE-TBX5^{mut} compared to that of control cells transfected with pHAGE-TBX5^{wt}, indicating that truncated TBX5 could inhibit the proliferation of HeLa cells, which is consistent with the results of a previous study (Goetz et al., 2006). Goetz et al. showed that TBX5 is important in controlling the length of the embryonic heart cell cycle, as its absence leads to cardiac cell cycle arrest in the late G1 or early S phase. The loss of TBX5 probably blocked cell cycle progression, thereby reducing in the number of cardiomyocytes, altering the timing of cardiac differentiation, and inducing defects in the formation of sarcomeres, ultimately leading to apoptosis. Interestingly, a previous study demonstrated that an alternatively spliced *Tbx5* transcript, with a 40 bp insertion at the 3' border of the T-box coding region, was detected in mouse heart and limbs. This transcript added four new residues after the 251st amino acid residue and a stop codon, thereby generating a C-terminal truncated *Tbx5* isoform (p. S252Rfs*5), *Tbx5b* (Georges et al., 2008). *Tbx5b* was primarily expressed in differentiated cells with a low proliferation rate both in vivo and in in vitro-cultured cells, and increased levels of *Tbx5b* were considered to cause growth arrest. Moreover, the inability of *Tbx5b* to activate the promoter of the natriuretic peptide A (*Nppa*) gene, a downstream target gene of *Tbx5*, was confirmed in cultured cardiomyocytes (Georges et al., 2008). The mutant truncated TBX5 protein (p. S252Rfs*2) in the present study was considerably similar to *Tbx5b* in terms of the amino acid sequence, indicating that the two proteins probably shared similar biological properties. Therefore, we hypothesized that the mutant truncated TBX5 protein reduced the proliferation of the cultured cells, probably owing to its limited capacity for activating the promoters of downstream target genes.

In summary, a novel *TBX5* c.755 + 1 G > A variant that caused abnormal mRNA splicing and enhanced the mRNA and protein expression of aberrant TBX5, was identified in the present study. The truncated TBX5 protein exhibited reduced nuclear localization and suppressed in vitro cell proliferation. Based on these results, we speculated that *TBX5* c.755 + 1 G > A may cause HOS through the following molecular mechanisms. First, the reduced nuclear localization of the truncated TBX5 protein moderated its binding to the promoter of downstream target genes, resulting in reduced transcription. Second, the loss of NID in truncated TBX5 protein inhibited its ability to bind to DNA or interact with other transcription factors, thereby decreasing the expression of downstream target genes, resulting in the functional inactivation of the TBX5 protein. Third, the truncated TBX5 protein inhibited cell proliferation and altered the normal proliferation and development patterns

in cardiomyocytes. Future studies are warranted to elucidate the molecular mechanism underlying HOS induced by *TBX5* c.755 + 1 G > A, with a focus on the truncated TBX5 protein and its binding to DNA, synergistic interactions with other proteins, and the expression of downstream target genes.

ACKNOWLEDGMENTS

The authors thank all family members of the proband for their kind cooperation and participation in the study.

CONFLICT OF INTEREST

The authors declare no conflict of interest.

AUTHOR CONTRIBUTIONS

De-Gang Wang performed the molecular analyses, interpreted the data, prepared the figures and tables, and wrote and submitted the manuscript. Xing-Sheng Dong contributed to the interpretation of clinical findings and performed the bioinformatics analyses and variants interpretation. Yi Xiong contributed to the collection of clinical data and the interpretation of clinical findings. Zhi-Ming Li contributed to the molecular analyses and critically revised the manuscript. Ying-Jun Xie and Shu-Hua Liang participated in the literature review and manuscript writing. Tian-Hua Huang designed, coordinated and supervised the study, and critically revised the manuscript. All authors have read and agreed to the published version of the manuscript.

DATA AVAILABILITY STATEMENT

The data that support the findings of this study are available from the corresponding author upon reasonable request.

ORCID

De-Gang Wang  <https://orcid.org/0000-0003-0059-4518>

REFERENCES

- Boogerd, C. J., Dooijes, D., Ilgun, A., Mathijssen, I. B., Hordijk, R., van de Laar, I. M., Rump, P., Veenstra-Knol, H. E., Moorman, A. F. M., Barnett, P., & Postma, A. V. (2010). Functional analysis of novel *TBX5* T-box mutations associated with Holt-Oram syndrome. *Cardiovascular Research*, 88(1), 130–139. <https://doi.org/10.1093/cvr/cvq178>
- Boogerd, C. J., & Evans, S. M. (2016). *TBX5* and NuRD divide the heart. *Developmental Cell*, 36(3), 242–244. <https://doi.org/10.1016/j.devcel.2016.02.011>
- Bruneau, B. G., Nemer, G., Schmitt, J. P., Charron, F., Robitaille, L., Caron, S., Conner, D. A., Gessler, M., Nemer, M., Seidman, C. E., & Seidman, J. G. (2001). A murine model of Holt-Oram syndrome defines roles of the T-box transcription factor *Tbx5* in cardiogenesis and disease. *Cell*, 106(6), 709–721. [https://doi.org/10.1016/s0092-8674\(01\)00493-7](https://doi.org/10.1016/s0092-8674(01)00493-7)
- Carvill, G. L., Heavin, S. B., Yendle, S. C., McMahon, J. M., O'Roak, B. J., Cook, J., Khan, A., Dorschner, M. O., Weaver, M., Calvert, S., Malone, S., Wallace, G., Stanley, T., Bye, A. M. E., Bleasel, A., Howell, K. B., Kivity, S., Mackay, M. T., Rodriguez-Casero, V., ... Mefford, H. C. (2013). Targeted resequencing in epileptic encephalopathies identifies de novo mutations in *CHD2* and *SYNGAP1*. *Nature Genetics*, 45(7), 825–830. <https://doi.org/10.1038/ng.2646>
- Chiavacci, E., Dolfi, L., Verduci, L., Meghini, F., Gestri, G., Evangelista, A. M., Wilson, S. W., Cremisi, F., & Pitto, L. (2012). MicroRNA 218 mediates the effects of *Tbx5a* over-expression on zebrafish

- heart development. *PLoS One*, 7(11), e50536. <https://doi.org/10.1371/journal.pone.0050536>
- ClinVar database. (2021). Retrieved from <https://www.ncbi.nlm.nih.gov/clinvar/?term=TBX5%5Bgene%5D>
- Collavoli, A., Hatcher, C. J., He, J., Okin, D., Deo, R., & Basson, C. T. (2003). TBX5 nuclear localization is mediated by dual cooperative intramolecular signals. *Journal of Molecular and Cellular Cardiology*, 35(10), 1191–1195. [https://doi.org/10.1016/s0022-2828\(03\)00231-1](https://doi.org/10.1016/s0022-2828(03)00231-1)
- Georges, R., Nemer, G., Morin, M., Lefebvre, C., & Nemer, M. (2008). Distinct expression and function of alternatively spliced Tbx5 isoforms in cell growth and differentiation. *Molecular and Cellular Biology*, 28(12), 4052–4067. <https://doi.org/10.1128/MCB.02100-07>
- Ghosh, T. K., Aparicio-Sánchez, J. J., Buxton, S., Ketley, A., Mohamed, T., Rutland, C. S., Loughna, S., & Brook, J. D. (2018). Acetylation of TBX5 by KAT2B and KAT2A regulates heart and limb development. *Journal of Molecular and Cellular Cardiology*, 114, 185–198. <https://doi.org/10.1016/j.yjmcc.2017.11.013>
- Ghosh, T. K., Packham, E. A., Bonser, A. J., Robinson, T. E., Cross, S. J., & Brook, J. D. (2001). Characterization of the TBX5 binding site and analysis of mutations that cause Holt-Oram syndrome. *Human Molecular Genetics*, 10(18), 1983–1994. <https://doi.org/10.1093/hmg/10.18.1983>
- Goetz, S. C., Brown, D. D., & Conlon, F. L. (2006). TBX5 is required for embryonic cardiac cell cycle progression. *Development*, 133(13), 2575–2584. <https://doi.org/10.1242/dev.02420>
- GTEX Consortium. (2020). The GTEx Consortium atlas of genetic regulatory effects across human tissues. *Science*, 369(6509), 1318–1330. <https://doi.org/10.1126/science.aaz1776>
- Guo, X., Lin, M., Yan, W., Chen, W., & Hong, G. (2019). A novel splice mutation induces exon skipping of the EXT1 gene in patients with hereditary multiple exostoses. *International Journal of Oncology*, 54(3), 859–868. <https://doi.org/10.3892/ijo.2019.4688>
- Hatcher, C. J., Goldstein, M. M., Mah, C. S., Delia, C. S., & Basson, C. T. (2000). Identification and localization of TBX5 transcription factor during human cardiac morphogenesis. *Developmental Dynamics*, 219(1), 90–95. [https://doi.org/10.1002/1097-0177\(200009\)219:1<90::AID-DVDY1033>3.0.CO;2-L](https://doi.org/10.1002/1097-0177(200009)219:1<90::AID-DVDY1033>3.0.CO;2-L)
- Hiroi, Y., Kudoh, S., Monzen, K., Ikeda, Y., Yazaki, Y., Nagai, R., & Komuro, I. (2001). Tbx5 associates with Nkx2-5 and synergistically promotes cardiomyocyte differentiation. *Nature Genetics*, 28(3), 276–280. <https://doi.org/10.1038/90123>
- Hug, N., Longman, D., & Cáceres, J. F. (2016). Mechanism and regulation of the nonsense-mediated decay pathway. *Nucleic Acids Research*, 44(4), 1483–1495. <https://doi.org/10.1093/nar/gkw010>
- IGSR. The International Genome Sample Resource. (2021). Retrieved from <https://www.internationalgenome.org/data-portal/search?q=12-114823280-C-T>
- Jang, J. W., Lee, W. Y., Lee, J. H., Moon, S. H., Kim, C. H., & Chung, H. M. (2011). A novel Fbxo25 acts as an E3 ligase for destructing cardiac specific transcription factors. *Biochemical and Biophysical Research Communications*, 410(2), 183–188. <https://doi.org/10.1016/j.bbrc.2011.05.011>
- Jeong, H. S., Jung, E. S., Sim, Y. J., Kim, S. J., Jang, J. W., Hong, K. S., Lee, W. Y., Chung, H. M., Park, K. T., Jung, Y. S., Kim, C. H., & Kim, K. S. (2015). Fbxo25 controls Tbx5 and Nkx2-5 transcriptional activity to regulate cardiomyocyte development. *Biochimica et Biophysica Acta*, 1849(6), 709–921. <https://doi.org/10.1016/j.bbaggm.2015.02.002>
- Kurosaki, T., & Maquat, L. E. (2016). Nonsense-mediated mRNA decay in humans at a glance. *Journal of Cell Science*, 129(3), 461–467. <https://doi.org/10.1242/jcs.181008>
- Lehner, R., Goharkhay, N., Tringler, B., Fasching, C., & Hengstschräger, M. (2003). Pedigree analysis and descriptive investigation of three classic phenotypes associated with Holt-Oram syndrome. *The Journal of Reproductive Medicine*, 48(3), 153–159.
- Li, H., & Durbin, R. (2009). Fast and accurate short read alignment with burrows-wheeler transform. *Bioinformatics*, 25(14), 1754–1760. <https://doi.org/10.1093/bioinformatics/btp324>
- Livak, K. J., & Schmittgen, T. D. (2001). Analysis of relative gene expression data using real-time quantitative PCR and the 2⁻(Delta Delta C(T)) method. *Methods*, 25(4), 402–408. <https://doi.org/10.1006/meth.2001.2534>
- Mele, M., Ferreira, P. G., Reverter, F., DeLuca, D. S., Monlong, J., Sammeth, M., Young, T. R., Goldmann, J. M., Pervouchine, D. D., Sullivan, T. J., Johnson, R., Segre, A. V., Djebali, S., Niarchou, A., Consortium, T. G., Wright, F. A., Lappalainen, T., Calvo, M., Getz, G., ... Guigo, R. (2015). Human genomics. The human transcriptome across tissues and individuals. *Science*, 348(6235), 660–665. <https://doi.org/10.1126/science.aaa0355>
- Merico, D., Spickett, C., O'Hara, M., Kakaradov, B., Deshwar, A. G., Fradkin, P., Gandhi, S., Gao, J., Grant, S., Kron, K., Schmitges, F. W., Shalev, Z., Sun, M., Verby, M., Cahill, M., Dowling, J. J., Fransson, J., Wienholds, E., & Frey, B. J. (2020). ATP7B variant c.1934T > G p. Met645Arg causes Wilson disease by promoting exon 6 skipping. *NPI Genomic Medicine*, 5, 16. <https://doi.org/10.1038/s41525-020-0123-6>
- Mori, A. D., & Bruneau, B. G. (2004). TBX5 mutations and congenital heart disease: Holt-Oram syndrome revealed. *Current Opinion in Cardiology*, 19(3), 211–215. <https://doi.org/10.1097/00001573-200405000-00004>
- Mori, A. D., Zhu, Y., Vahora, I., Nieman, B., Koshiba-Takeuchi, K., Davidson, L., Pizard, A., Seidman, J. G., Seidman, C. E., Chen, X. J., Henkelman, R. M., & Bruneau, B. G. (2006). Tbx5-dependent rheostatic control of cardiac gene expression and morphogenesis. *Developmental Biology*, 297(2), 566–586. <https://doi.org/10.1016/j.ydbio.2006.05.023>
- Naiche, L. A., Harrelson, Z., Kelly, R. G., & Papaioannou, V. E. (2005). T-box genes in vertebrate development. *Annual Review of Genetics*, 39, 219–239. <https://doi.org/10.1146/annurev.genet.39.073003.105925>
- Newbury-Ecob, R. A., Leanage, R., Raeburn, J. A., & Young, I. D. (1996). Holt-Oram syndrome: A clinical genetic study. *Journal of Medical Genetics*, 33(4), 300–307. <https://doi.org/10.1136/jmg.33.4.300>
- Park, C. M., & Xian, M. (2015). Use of phosphorodithioate-based compounds as hydrogen sulfide donors. *Methods in Enzymology*, 554, 127–142. <https://doi.org/10.1016/bs.mie.2015.05.002>
- Pohl, C., & Dikic, I. (2019). Cellular quality control by the ubiquitin-proteasome system and autophagy. *Science*, 366(6467), 818–822. <https://doi.org/10.1126/science.aax3769>
- Qin, L., Wang, J., Tian, X., Yu, H., Truong, C., Mitchell, J. J., Wierenga, K. J., Craigen, W. J., Zhang, V. W., & Wong, L. C. (2016). Detection and quantification of mosaic mutations in disease genes by next-generation sequencing. *The Journal of Molecular Diagnostics*, 18(3), 446–453. <https://doi.org/10.1016/j.jmoldx.2016.05.002>
- Qiu, C., Li, C., Tong, X., Dai, L., Liu, W., Xie, Y., Zhang, Q., Yang, G., & Li, T. (2020). A novel TSC1 frameshift mutation c.1550_1551del causes tuberous sclerosis complex by aberrant splicing and nonsense-mediated mRNA degradation (NMD) simultaneously in a Chinese family. *Molecular Genetics & Genomic Medicine*, 8(10), e1410. <https://doi.org/10.1002/mgg3.1410>
- Richards, S., Aziz, N., Bale, S., Bick, D., Das, S., Gastier-Foster, J., Grody, W. W., Hegde, M., Lyon, E., Spector, E., Voelkerding, K., Rehm, H. L., & ACMG Laboratory Quality Assurance Committee. (2015). Standards and guidelines for the interpretation of sequence variants: A joint consensus recommendation of the American College of Medical Genetics and Genomics and the Association for Molecular Pathology. *Genetics in Medicine*, 17(5), 405–424. <https://doi.org/10.1038/gim.2015.30>
- Shan, J., Pang, S., Qiao, Y., Ma, L., Wang, H., Xing, Q., Wanyan, H., Wu, G., & Yan, B. (2012). Functional analysis of the novel sequence variants within TBX5 gene promoter in patients with ventricular septal defects. *Translational Research*, 160(3), 237–238. <https://doi.org/10.1016/j.trsl.2012.04.003>
- Smemo, S., Campos, L. C., Moskowitz, I. P., Krieger, J. E., Pereira, A. C., & Nobrega, M. A. (2012). Regulatory variation in a TBX5 enhancer leads

- to isolated congenital heart disease. *Human Molecular Genetics*, 21(14), 3255–3263. <https://doi.org/10.1093/hmg/dds165>
- Spinner, N. B., & Conlin, L. K. (2014). Mosaicism and clinical genetics. *American Journal of Medical Genetics. Part C, Seminar Medical Genetics*, 166C(4), 397–405. <https://doi.org/10.1002/ajmg.c.31421>
- The Genome Aggregation Database. (2021). Retrieved from http://gnomad-sg.org/variant/12-114823280-C-T?dataset=gnomad_r3
- The Human Gene Mutation Database. (2021). Retrieved from <http://www.hgmd.cf.ac.uk/ac/gene.php?gene=TBX5>
- Tyburczy, M. E., Dies, K. A., Glass, J., Camposano, S., Chekaluk, Y., Thorner, A. R., Lin, L., Krueger, D., Franz, D. N., Thiele, E. A., Sahin, M., & Kwiatkowski, D. J. (2015). Mosaic and intronic mutations in TSC1/TSC2 explain the majority of TSC patients with no mutation identified by conventional testing. *PLOS Genetics*, 11(11), e1005637. <https://doi.org/10.1371/journal.pgen.1005637>
- Vanlerberghe, C., Jourdain, A. S., Ghoumid, J., Frenois, F., Mezel, A., Vaksman, G., Lenne, B., Delobel, B., Porchet, N., Cormier-Daire, V., Smol, T., Escande, F., Manouvrier-Hanu, S., & Petit, F. (2019). Holt-Oram syndrome: Clinical and molecular description of 78 patients with TBX5 variants. *European Journal of Human Genetics*, 27(3), 360–368. <https://doi.org/10.1038/s41431-018-0303-3>
- Wang, F., Liu, D., Zhang, R. R., Yu, L. W., Zhao, J. Y., Yang, X. Y., Jiang, S. S., Ma, D., Qiao, B., Zhang, F., Jin, L., Gui, Y. H., & Wang, H. Y. (2017). A TBX5 3'UTR variant increases the risk of congenital heart disease in the Han Chinese population. *Cell Discovery*, 3, 17026. <https://doi.org/10.1038/celldisc.2017.26>
- Wang, Y., Sun, Y., Liu, M., Zhang, X., & Jiang, T. (2019). Functional characterization of Argininosuccinate Lyase gene variants by mini-gene splicing assay. *Frontiers in Genetics*, 10, 436. <https://doi.org/10.3389/fgene.2019.00436>
- Wei, X., Ju, X., Yi, X., Zhu, Q., Qu, N., Liu, T., Chen, Y., Jiang, H., Yang, G., Zhen, R., Lan, Z., Qi, M., Wang, J., Yang, Y., Chu, Y., Li, X., Guang, Y., & Huang, J. (2011). Identification of sequence variants in genetic disease-causing genes using targeted next-generation sequencing. *PLoS One*, 6(12), e29500. <https://doi.org/10.1371/journal.pone.0029500>
- Willis, M. S., Townley-Tilson, W. H., Kang, E. Y., Homeister, J. W., & Patterson, C. (2010). Sent to destroy: The ubiquitin proteasome system regulates cell signaling and protein quality control in cardiovascular development and disease. *Circulation Research*, 106(3), 463–478. <https://doi.org/10.1161/CIRCRESAHA.109.208801>
- World Medical Association. (2013). World Medical Association Declaration of Helsinki: Ethical principles for medical research involving human subjects. *Journal of the American Medical Association*, 310(20), 2191–2194. <https://doi.org/10.1001/jama.2013.281053>
- Yi, C. H., Russ, A., & Brook, J. D. (2000). Virtual cloning and physical mapping of a human T-box gene, TBX4. *Genomics*, 67(1), 92–95. <https://doi.org/10.1006/geno.2000.6222>
- You, K. T., Li, L. S., Kim, N. G., Kang, H. J., Koh, K. H., Chwae, Y. J., Kim, K. M., Kim, Y. K., Park, S. M., Jang, S. K., & Kim, H. (2007). Selective translational repression of truncated proteins from frameshift mutation-derived mRNAs in tumors. *PLoS Biology*, 5(5), e109. <https://doi.org/10.1371/journal.pbio.0050109>
- Zaragoza, M. V., Lewis, L. E., Sun, G., Wang, E., Li, L., Said-Salman, I., Feucht, L., & Huang, T. (2004). Identification of the TBX5 transactivating domain and the nuclear localization signal. *Gene*, 330, 9–18. <https://doi.org/10.1016/j.gene.2004.01.017>

SUPPORTING INFORMATION

Additional supporting information may be found in the online version of the article at the publisher's website.

How to cite this article: Wang, D.-G., Dong, X.-S., Xiong, Y., Li, Z.-M., Xie, Y.-J., Liang, S.-H., & Huang, T.-H. (2021). Identification of a novel TBX5 c.755 + 1 G > A variant and related pathogenesis in a family with Holt–Oram syndrome. *American Journal of Medical Genetics Part A*, 188A:58–70. <https://doi.org/10.1002/ajmg.a.62488>